ICAST2014 082

Design and Simulation of Morphing Airfoil Sections with SMA Actuators for Wind Turbine Rotors

Karakalas A.[1], Machairas T.[1], Solomou A.[1], Riziotis V.[2] and Saravanos D.[1*]

[1] Mechanical Engineering and Aeronautics Department, University of Patras, Patras, Greece
[2] Mechanical Engineering Department, National Technical University of Athens, Athens, Greece

Abstract

The paper presents on-going work conducted on extreme and cyclic aerodynamic load alleviation of wind turbine blades (WTB) using morphing blade sections. Promising morphing concepts considering either mechanisms or a continuously deforming airfoil structure are studied in detail. Antagonistic shape memory alloy (SMA) wire/rod actuators are investigated in order to deflect the morphing trailing edge (TE) section both upwards and downwards. A morphing section of a WTB is first designed to follow target airfoil shape profiles which yield prescribed changes in the lift coefficient. Subsequently, the morphing airfoil is designed to follow prescribed target time trajectories with the aid of a PID controller, based on time series data relating the trailing edge movement with the time variation of the lift coefficient obtained through aeroelastic analyses. The thermomechanically coupled time response of the morphing section is simulated using specialty finite element models. The development of the morphing WTB section revealed several challenges. These include the enhancement of the slow response of SMA actuators, the retainment of stresses and power within reasonable limits and the minimization of tracking error. A PID controller is described and optimized to achieve fast actuator response through optimized cooling and heating cycles. Numerical results quantify the trailing edge angular movement, the time response of the morphing section and the developed stresses in the actuators. Estimations of the achieved variations of lift coefficient vs. time are also presented to assess the aerodynamic performance of the morphing section.

1. INTRODUCTION

The tremendous upscaling of wind turbine rotors observed over the last decades is motivated by the need to increase the power generation capacity, maximize site usage, take advantage of potentially greater wind speed and lower turbulence at higher altitudes, and finally reduce the cost of produced energy per kilowatt-hour (kWh). The improvement of wind turbines to become the most competitive renewable energy source is a key objective of the European Union wind industry's research and development (1). Yet, the design of flexible light-weight rotors with diameters exceeding 160 m subjected to higher aerodynamic loads is challenging, because of the induced high extreme and cyclic stresses in the blade structure and the reduction of fatigue life. The implementation of innovative active load alleviation concepts using blade sections which can change their shape and curvature may offer a solution to decrease cyclic stresses, improve fatigue life of the rotor, and subsequently decrease the overall cost of other wind turbine components (tower, drive train, shaft, drives etc.), the maintenance and off-duty time costs (2).

* Corresponding author, email:saravanos@mech.upatras.gr

The forces acting on the rotor of a wind turbine are attributable to the effects of aerodynamic, gravitational and inertial forces. The different loads and stresses can be classified either according to their effect with time on the rotating rotor or can be generally divided into two main categories: ultimate (extreme) loads and fatigue loads due to turbulence, operating in yawed conditions, shear flow and the effect of the tower (3) (4). The main focus of present work is on fatigue load alleviation to reduce fatigue damage from the latter fluctuating loads, as fatigue life is a key factor for the design of wind turbine blades.

Research aimed in this area is mainly focused on developing new technologies and/or using materials in an innovative way to successfully reduce ultimate and fatigue loads on wind turbines. Principally, there exist two methods to control loading of wind turbine blades: passive and active control. In the former case, the rotor blades are passively adapted through their aero-elastic response to the aerodynamic loads. Passive load control methods mainly include blades with bend-twist coupling (5) (6), blades with sweeping capabilities (7) and use of multi-stable composites (8). In the case of active load control, the aerodynamic properties of a blade section are adjusted using specially designed mechanisms and/or active materials embedded in the structure (9) to adapt the blade profile at any span-wise location in response to the wind environment (10). Some of the reported methods include individual blade pitch control (11), yaw systems (12), actively controlled microtabs (similar to Gurney flaps) (13), use of adaptive trailing edge geometry (14), compliant trailing edges (15), and so forth.

The present paper presents the design and simulation of morphing blade sections, which can change their curvature using articulated mechanisms with shape memory alloy (SMA) actuators. The paper is organized as follows: the fundamental SMA material behavior and corresponding constitutive models are summarized. Numerical models of the morphing section are presented using a specialty finite element capable to model the transient thermomechanical response of SMA actuators (16). Various morphing section concepts with articulated trailing edge mechanisms are analyzed to produce airfoil target shapes which result in predefined changes of the lift coefficient. Subsequently, the heating and cooling cycles of the shape memory alloy actuators are controlled through an optimized PID regulator, such that the morphing section movement follows a precalculated time series of target shapes (target trajectory) producing lift coefficients which reduce the variation of the aerodynamic loads applied on the section. Numerical results quantify the capability of a WTB morphing section to yield specific load alleviation trajectories, and identify the key parameters which may limit the frequency and amplitude range of its response.

2. SHAPE MEMORY ALLOY ACTUATORS

The constant demand for materials with disruptive properties (for example sensing and actuation) that satisfy stringent structural requirements and provide additional engineering functionality has led to the insertion of a new branch of materials called multifunctional materials. Shape memory alloys fall in this category possessing the unique property of shape recovery when certain thermomechanical loading is applied (17). Shape memory alloys are selected as potential actuators because they exhibit large stroke due to the high induced strains, high energy density and subsequently high actuation power density and require low energy voltage (compared to conventional electric motors).

2.1 Description of Shape Memory Alloys Behavior

Shape memory alloys exhibit an inherent ability to recover strain and shape when temperature increases above a critical threshold. This unique behavior of shape recovery is related with a diffusionless phase transformation between two different phases, the high temperature austenitic phase (Austenite – A) and the lower temperature martensitic phase (Martensite – M). The latter can be met either in twinned (M^t) or in detwinned/reoriented (M^d) form. In the absence of mechanical load and upon cooling, the phase transition from austenite to twinned martensite is called forward transformation. Direct transformation of austenite to detwinned martensite through mechanical loading is accompanied by large inelastic macroscopic strain (depending on the alloy, around 4%) that is not recovered upon unloading. If the material is heated above a temperature threshold it transforms back to austenite and this procedure is associated with shape change to parent configuration. The procedure is called shape memory effect (SME). Actuation capabilities of shape memory alloys are presented when the material exhibits shape memory effect. Another special behavior exhibited by shape memory alloys is called pseudoelasticity. This behavior effectively contributes to their functionality as actuators under high temperature environments and is associated with recovery of transformation strain at these conditions. While the shape memory effect is exhibited at low temperature conditions (below M_f), the pseudoelastic effect is exhibited at high temperatures (above A_f). **Figure 1** presents schematically the SME and the pseudoelastic effect in the stress – strain – temperature space. In the diagram the symbol ξ indicates the martensitic volume fraction (MVF). As it is represented in **Figure 1** the forward and reverse transformation during a complete pseudoelastic cycle result in the formation of a hysteresis loop, which represents the energy dissipated during the transformation cycle. The constitutive model of Lagoudas et al. (18) in a properly reduced 2D form was selected to describe the previously thermodynamic state and behavior of the material.

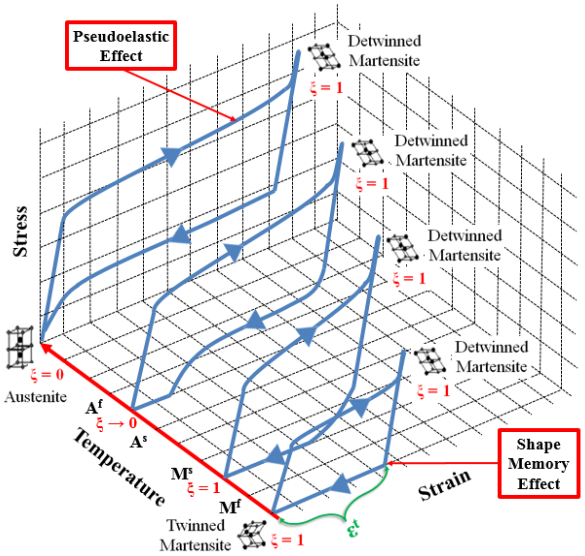

Figure 1. Stress – Strain – Temperature Space

2.2 Numerical Tool for Simulating SMA Actuator Behavior

Morphing structures with shape memory alloy actuators exhibit complex response under various thermal, mechanical, or thermomechanical loading conditions. A numerical tool enabling prediction of the SMA actuator and morphing structure response has been developed and applied in the simulation analyses. The core of the aforementioned numerical tool is a new beam finite element, capable to predict both the coupled thermomechanical behavior of the actuators in 2D form and their time

response (16). The developed finite element is implemented in the framework of Finite Element Analysis (FEA) software ABAQUS available User Element (UEL) subroutine (19). The subroutine receives as input the element nodal translations and temperatures, as well as some other element information, for the calculation of strain and temperature at integration points. Calculated variables are sent to a user material subroutine (UMAT) where axial and shear stresses, material Jacobian matrix of the constitutive model, the volumetric heat generation, the variation of the axial stress with respect to the temperature, the variation of volumetric heat generation with respect to the axial strain, the variation of volumetric heat generation with respect to the temperature and updated state variables are calculated. After the calculation of element contribution on the tangent matrix and nodal residual load vector, output, which include element nodal residual load vector, tangent matrix and the updated state variables, is passed to the global implicit Newton-Raphson solver.

Along with the thermomechanical response of the shape memory beam actuator, the specialty beam finite element is capable of predicting the heat conduction through-the-thickness and along the axis of the actuator and the heat losses. Therefore, the required power to elevate the temperature of the material is calculated. Knowing explicitly the effect of power in the thermal state of the material, it is possible to control the transformation, and subsequently the actuation time response of the shape memory alloy actuators which is dictated primarily by the specific heat capacity and depends on the rate of temperature change. It is clear that the amount of heating energy provided to the actuators in order to elevate their temperature and the surface convection conditions play a significant role to the response of the morphing mechanism, as they drive the actuator temperature and the exerted actuation strains. Consequently, the applied heating power and the convection conditions are the quantities that should be controlled in order to achieve the desired morphing time response.

3. MORPHING CONCEPT WITH SHAPE MEMORY ALLOY ACTUATORS

Morphing has been used in the field of aeronautics to identify aircraft components, e.g. wing trailing and leading edges, winglets, engine nozzles which can undergo large geometrical changes to enhance or adapt to various mission profiles. In the case of wind turbine rotors, the term morphing refers to geometrical changes in the upper and lower aerodynamic surfaces affecting the lift coefficient (C_L) and altering the aerodynamic loads acting on the airfoil. The morphing of an airfoil shape in a controlled and continuous manner causes the lift coefficient to alter with respect to the aerodynamic loads produced by variations in wind speed, hence, load alleviation can be achieved.

In the framework of the present work the airfoil section between 70 and 80% span of an 86m blade of a horizontal axis wind turbine (HAWT) was properly modified with the implementation of a morphing mechanism activated by shape memory alloy wire actuators. The original blade and airfoil geometry and the required information about the materials were provided by DTU Wind Energy Institute (20). Information about the target shapes of the airfoil and the trajectories that should be followed to achieve aerodynamic load alleviation were calculated by the National Technical University of Athens (NTUA) using appropriate filters and a PID control loop, aiming to reduce the blade fatigue loads by changing the coefficient of lift in normal operation. The controller loop (**Figure 2**) receives feedback input from either a load sensor (strain gauge) at the root of the blade or an accelerometer at the blade tip and produces an output signal as input for actuators activation control.

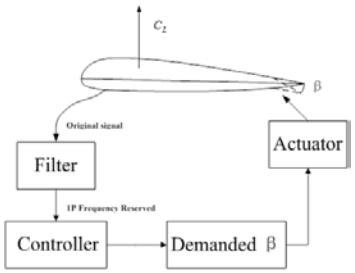

Figure 2. Flow Diagram of NTUA Control Loop

3.1 Aerodynamic Load Alleviation

Aeroelastic analysis performed by NTUA referred to a typical 2D blade section model from a three blade horizontal axis 10 MW wind turbine. The design of the cross sectional shape along the blades was based on the FFA-W3-xxx airfoil family equipped with Gurney flaps to increase aerodynamic performance. The selected airfoil lies between 70 and 80% of total blade length (≈ 86m in pre bent shape) where the aerodynamic loads are expected to maximize. For the purpose of calculating aerodynamic characteristics of the deformable airfoil a 2D free wake viscous-inviscid interaction code (21) was utilized, while the structural response was simulated with concentrated spring properties in the flapwise, chordwise and torsional direction of motion (22).

Filtering of the input signal is performed in order to maintain at least the 1P frequency of 0.16 Hz which is mainly responsible for the fatigue loads acting on the blade. This frequency corresponds to a period of 6.25 seconds which reflects on the blade aerodynamic loading and accelerations. Depending on the sensor used, the filtered signal is passed through a PI or PD control and the required flap angle time-series is determined as an output. The flap-angle time-series are used as input to determine the deflection or morphing of the airfoil. It should be noted that aerodynamic load alleviation is expressed as the produced variation of the airfoil lift coefficient when target angular rotation of the equivalent flap is achieved.

3.2 Airfoil Target Shapes

In this study, morphing mechanisms are considered in the section or the airfoil between the shear web and the trailing edge (TE). **Figure 3a** identifies the main parameters defining the shape change of the airfoil (percent of the chord length with moving ability d and rotation angle β of the TE) and Figure 2b illustrates schematically how the combination of the moved chord section and TE rotation angle affects the variation of the lift coefficient.

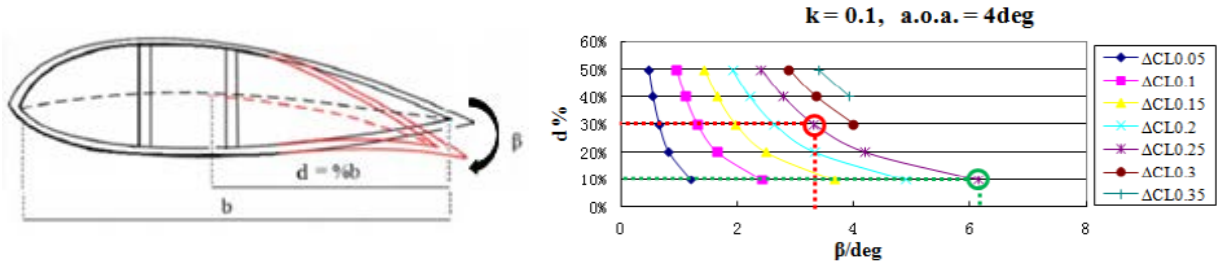

(a) **(b)**

Figure 3. Morphing Concept and its Effect on ΔC_L
(a) Variables used for Morphing Shape Definition
(b) Diagram Relating Percent of Chord Length Morphed and Angular Rotation with ΔC_L

The range of morphing parameters d and β was defined for a given reduced frequency k and angle of attack (A.o.A) based on airfoil data provided by NTUA. As depicted in **Figure 3b**, a certain variation in lift coefficient can be obtained by various combinations of variables d and β. For example, a variation in lift coefficient of 0.25 is produced when d = 30% and β = 3.2˚ (represented by the red cycle in **Figure 3b**). To achieve the same variation in lift coefficient, ΔC_L=0.25, with another combination of the variables d and β, it is necessary to move to another point on the same curve, i.e. to morph 10% of chord length with an angular rotation of 6.1º (represented by green cycle in **Figure 3b**).

3.3 Design of Trailing Edge Morphing Concepts

The analysis and design of the airfoil was performed with FEA using ABAQUS. The original section consisted of eleven regions, each one of them is constructed with composite materials of a defined layup sequence. Each part of every region was modeled with 8-node shell elements of quadratic geometric order and 6 degrees of freedom per node. Airfoil section assembly was created by joining the proper parts together with tie constrains.

Shape memory alloy actuators were embedded into the airfoil's trailing edge and mounted either on rigid truss structures or on mechanism parts. Among the various designs of the concepts analyzed the rib mechanism shown in **Figure 4** consisting of 3D solid parts with slotted skin proved to be more promising and feasible. In the figure the shape memory alloy actuators are highlighted in red colour

The use of a 3D rib mechanism with slotted skin, offers the opportunity to predefine the morphing shape and to control it in a more precise and predicted manner. The mechanism's weight can be adjusted by proper selection of materials, for example, the main parts of the mechanism may be constructed from foam, composite materials, sandwich material structures etc. The rigidity of the trailing edge is practically dominated by the actuators stiffness. Finally, the slotted ribs offer the opportunity to use flexible skin materials to bridge the gaps of the slots and provide continuous aerodynamic surfaces and additionally control the shape of the morphed airfoil.

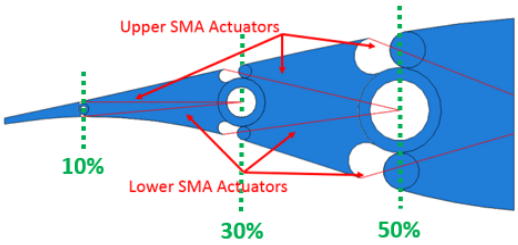

Figure 4. Trailing Edge Morphing Design Concepts with Rib Mechanism Structure

The selected TE morphing mechanism concept consists of three moving parts connected with hinged pins at 10%, 30% and 50% of chord length and six shape memory alloy actuators (2 antagonistic wire actuators for each part) as it is presented in **Figure 4**. The undeformed configuration coincides with airfoil's original – undeformed shape and each one of the three pins between the moving parts is located on airfoil's camber line so that upon actuation the center of rotation is known and the pin remains on the camber line even after the airfoil is morphed. The antagonistic shape memory alloy actuators enable both upwards and downwards movement of the airfoil. Furthermore, the particular mechanism design allows the independent move of each part or their combination thus resulting in a variety of morphing shapes.

3.4 Idealized Target Trajectory

In order to study the adequacy of the time response of shape memory alloy actuators and, subsequently, of the morphing airfoil, an idealized sinusoidal input target trajectory was produced. The basis of this trajectory was a time series provided by NTUA for the alleviation of aerodynamic loads which associates the angular movement of a flap, with a center of rotation at 10% of chord length. The time series is shown in **Figure 5**. Using the calculated dominant frequency and the maximum amplitude of the stochastic input signal, the following sinusoidal signal for the rotation angle was produced $3.6 \cdot \sin\left(\frac{2 \cdot \pi}{6.25} \cdot t + \pi\right)$. This ideal signal was used as target trajectory for the investigations conducted on the feasibility of the morphing rib mechanism to achieve the corresponding frequency, amplitude and to finally track the angle trajectory implementing a PID controller.

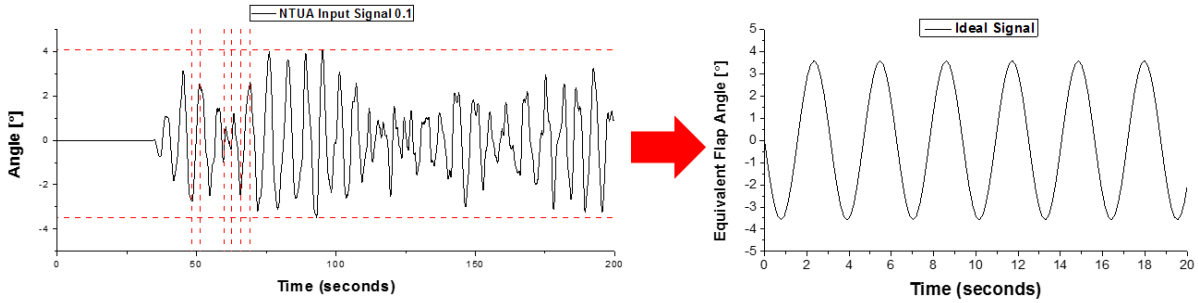

Figure 5. Actual Signal (left) and extracted Ideal Sinusoidal Signal (right)

3.5 Implementation of Actuator PID Control

A Proportional – Integral – Derivative (PID) controller was adopted to control the position of the morphing mechanism using the shape memory alloy wire actuators. The target of the controller (R_0) is the angular rotation angle β (t). The error between the desired set point and the measured variable by the sensor, is estimated in a feedback loop and minimized by the controller algorithm which entails three constant gain parameters. These parameters affect the output response (in our case the applied thermal load on the actuators) and are commonly termed as the proportional gain (k_p), which acts on the preset error, the integral gain (k_i), which acts on the history of error variation and the derivational gain (k_d), which acts on the pace of error changes as a prediction of future error changes. The weighted sum of these parameters is used to adjust the process via a control element. Because of the highly nonlinear response of the actuators, a custom made subroutine was developed which is interacting with the UEL subroutine in the FEA global solver. The flow diagram of the controller operation is presented in **Figure 6**.

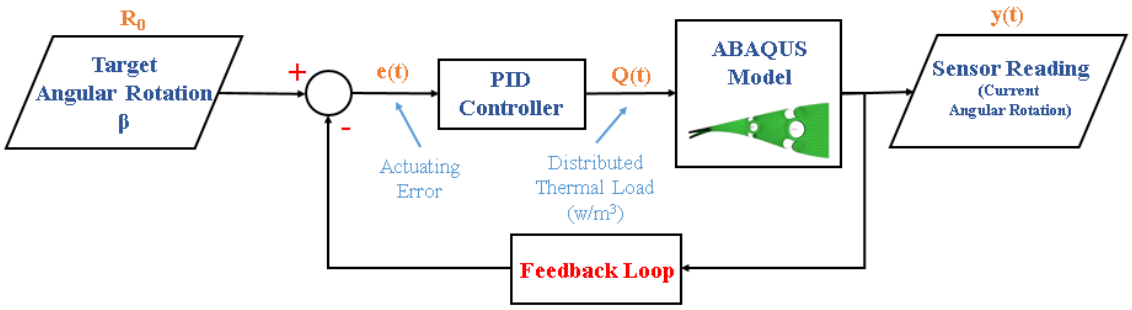

Figure 6. Flow Diagram of the Shape Memory Alloy Actuator Controller

4. SIMULATION RUNS FOR PERFORMANCE EVALUATION

Based on **Figure 3b** and the considered configuration of the morphing mechanisms shown in **Figure 4**, there exist a variety of ways to deflect the airfoil, each one having a specific impact on the aerodynamic performance of the airfoil and the actuators. Without loss of generality, this study focusses on the movement of the last rib of the mechanism which corresponds to 10% of chord length. The TE rib mechanism with the embedded actuators is modelled in ABAQUS. The FE model was built using 8-node 3D linear brick reduced integration elements for the parts of the mechanism, the structural parts of the airfoil were modeled with 8-node shell elements and the shape memory alloy actuators were modeled using the 2-node specialty beam finite element to simulate the actuator

thermomechanical and time response. Initial FEA analyses were performed to assess the mechanism functionality without taking into account time effects and illustrated that thermal loading in form of temperature increase from 310K to 350K of the proper actuator (upper or lower) results in respective mechanism movement in the desirable direction (upwards or downwards) to the desirable target angle $\beta=3.6^{o}$. This quantitative approach demonstrated the range of shape morphing capabilities performed under predefined thermal conditions of the actuators.

4.1 Idealized Input Trajectory Time Response

After the promising results of this preliminary study, the morphing capability of the mechanism to follow the predefined input time trajectories of angle β shown in **Figure 5** was investigated. Assuming an ambient temperature of 295K, the movement of the TE was simulated manually turning on and off the Joule energy applied on the actuators at the peak of each cycle. As it can be observed in **Figure 7**, the mechanism reaches the peak positions but follows the trajectory with substantial error. Additional unforeseen challenges raised from the simulations are the high stresses developed in actuators and the high temperature levels. In **Figure 8**, the predicted actuators axial stress tends to saturate to values over 800 MPa, above the 650 MPa material yield strength. It is also clear from **Figure 9** that the actuator temperature saturates in a region between 420 and 460K. Furthermore, the martensitic volume fraction (MVF) shown in **Figure 10** tend to saturate between 0.3 and 0.5, so reverse transformation and return to fully martensitic phase (MVF = 1) cannot be achieved unless the temperature is dramatically lowered.

The gradual increase of stress and temperature and the decrease of MVF occurs because the heated (activated) shape memory alloy actuator does not have sufficient time to cool and return to its initial state before the antagonistic actuator is activated. Consequently, in order to move the flap in the opposite direction, the antagonistic actuator should apply higher forces, thus resulting in higher stresses on both actuators. Increased stress levels lead to increased transformation temperature thresholds, thus more heat energy is required to reach the thresholds and complete the required transformation for strain production.

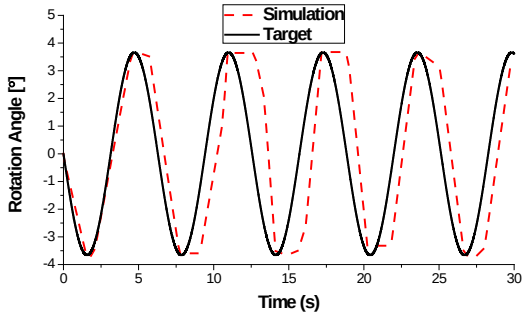

Figure 7. Flap Angular Rotation vs. Time

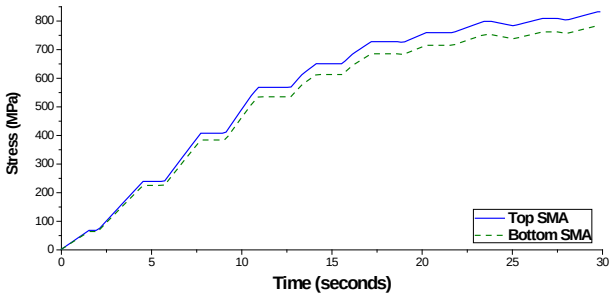

Figure 8. Actuators Stress vs. Time

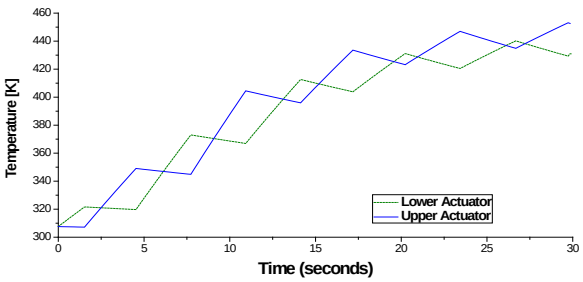

Figure 9. Actuators Temperature vs. Time

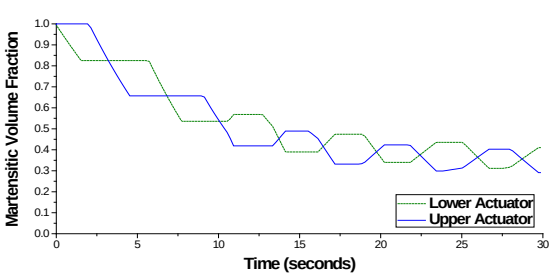

Figure 10. Actuators MVF vs. Time

4.2 Optimizing Actuator Performance

To overcome the previous challenges, the following improvements were considered. First, conditions of active cooling were introduced in the simulation by adjusting the value of the heat convection coefficients. Free heat convection depends on the temperature difference between the actuators and the ambient temperature. If the ambient temperature or the temperature near the actuators is lowered below the temperature of the environment heat convection will be enhanced. Then, the initial martensitic volume fraction of the shape memory actuators was adjusted such that to shift the phase transformation in the actuators in the regime where the rate of transformation strain vs. temperature change exhibits the highest values. Instead of setting the actuators, during the initial configuration of the mechanism, in fully martensitic phase, they were set at a MVF=20%. This practice enables the transformation to happen in a more narrow temperature range and result in a faster response with less energy requirements. Thus, lower temperature changes will lead to the same effect on the transformation strain. With this modification the resistance from antagonistic SMA wire is reduced, as transformation will occur to absorb elastic energy and therefore the required actuation force by the active actuator will decrease. Another benefit is that lower temperature changes will lead to the same effect on the transformation. The last improvement was the inclusion of an optimized PID controller.

Figure 11 presents the simulated flap rotational angle trajectory of the morphing airfoil vs. the input target trajectory, after the previous improvements were implemented. It is clear that the optimization of the shape memory alloy actuator operation has substantially improved the error between the achieved trajectory and the target one. It should be noted that the small deviations near the peaks of the trajectory can be further reduced with advanced optimization of the PID controller.

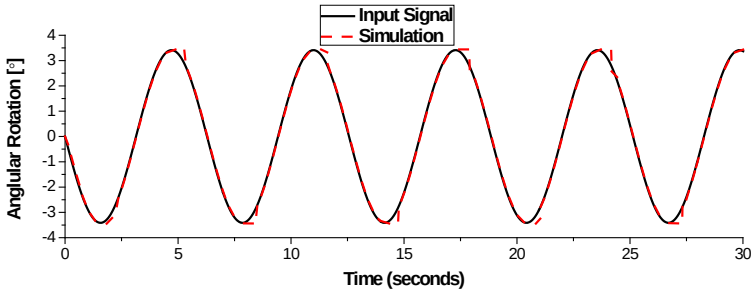

Figure 11. Equivalent Flap Angle vs. Time

More interesting are the predicted dramatic reduction in developed actuator stresses and temperatures presented in **Figure 12** and **Figure 13**, respectively. Regarding the stress levels, it can be safe to assume that stress will saturate to very low levels (below 30 MPa, mean value 24÷26 MPa) providing an extended fatigue life for the shape memory alloy actuators. The required temperature difference of about 20K, between the values of 326K and 347K, leads to reduced heating input energy requirements, rendering the optimized actuators much faster and more energy efficient. It is also clear that the variation of MVF is limited between 0.15÷0.27. This leads to fast transitions between the desired transformation states of the actuator. Variation of MVF during simulation time is presented in **Figure 14**. **Figure 15** presents the power applied by the PID controller to each of the two shape memory alloy actuators with respect to time. The required power is less than 165 W and is applied only for short intervals of time. In closing, the previous results have demonstrated: 1. that it is feasible for the morphing airfoil to reach the 1P frequency of the wind turbine blade through proper actuator optimization; 2. the described improvements in the actuator time response enhance, reduce the tracking error between the morphing airfoil motion and the target trajectory, but most importantly retain the stress, temperature and input power at very low limits.

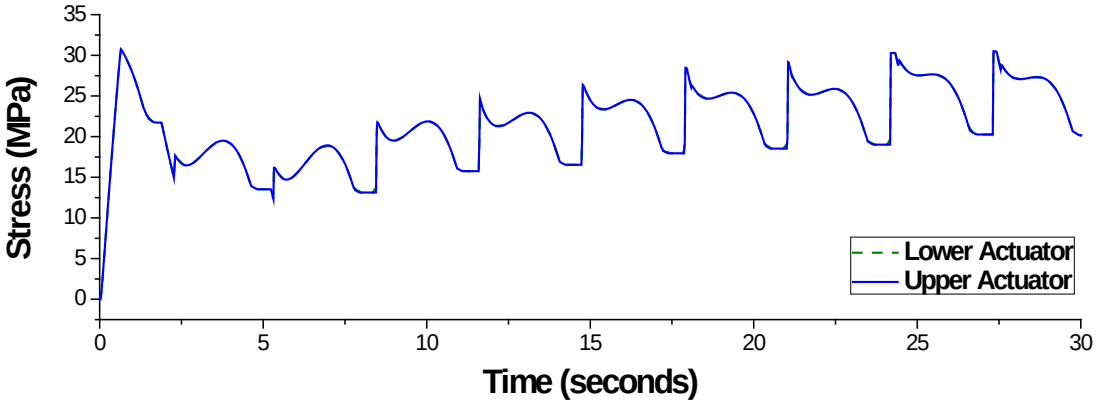

Figure 12. Actuators Stress vs. Time

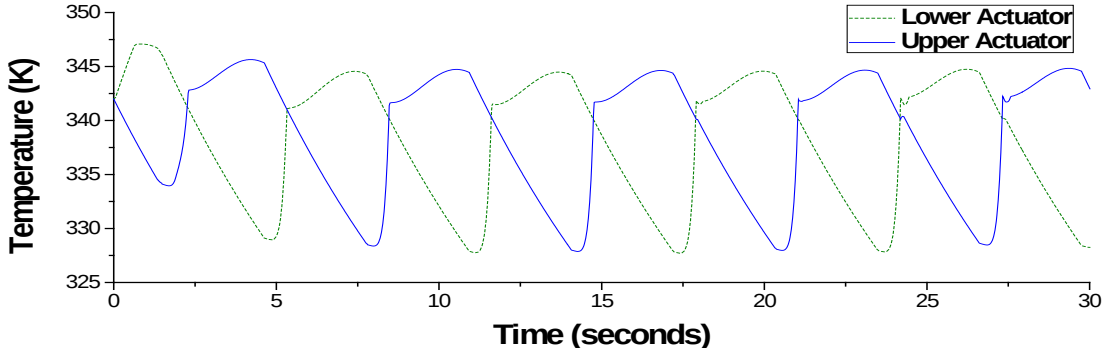

Figure 13. Actuators Temperature vs. Time

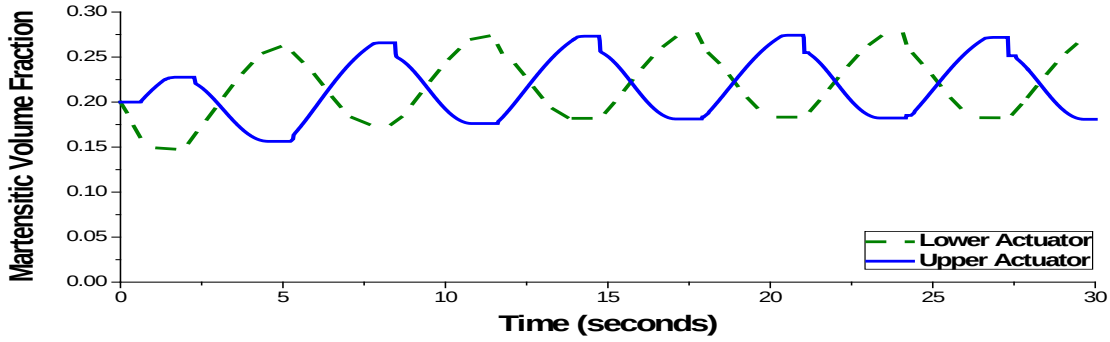

Figure 14. Actuators Martensitic Volume Fraction vs. Time

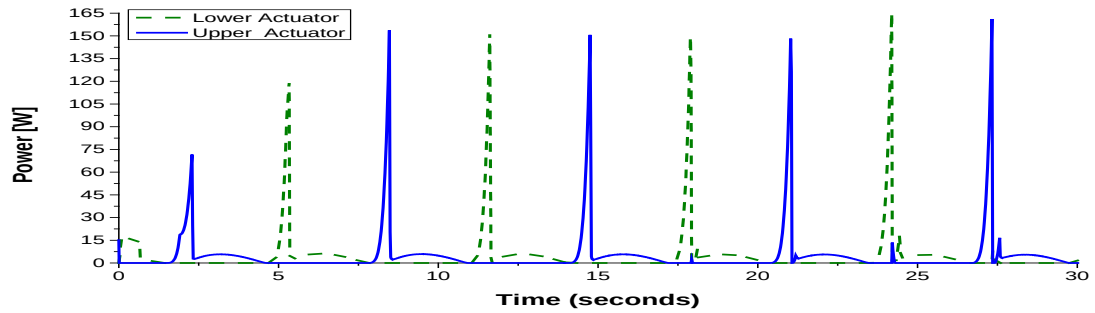

Figure 15. Power Consumed for Actuating Shape Memory Alloy Wires

SUMMARY AND CONCLUSIONS

This paper briefly presents the design and implementation of shape memory alloy actuators in an articulated rib mechanism of a morphing wind turbine blade section. The mechanism moving parts driven by the actuators change the original airfoil's shape in a continuous manner according to a predefined target shape in order to achieve the alleviation of aerodynamic loads. FEA modelling and time simulations of the complex thermomechanical behaviour of the shape memory alloy actuators for the airfoil morphing were presented using a specialty beam finite element. The morphing airfoil models subsequently included the interactions with a PID controller for controlling the actuators response.

Although the presented methodology and the morphing mechanism configuration offers the opportunity to study a variety of target shapes, the numerical analysis and results were focused on the effect of movement of 10% chord length at the airfoil trailing edge of a 10 MW horizontal axis wind turbine blade. An effectively active flap of the mechanism was simulated to demonstrate the abilities of the concept and the physical limitation.

Taking into consideration parameters for optimizing actuators' performance it was proved possible to follow an ideal sinusoidal trajectory of the flapping angle at the 1P frequency. The optimization of the actuators operation was achieved by choosing the phase transformation region (regarding initial and final MVF) and active cooling embedded in a PID controller. The optimization processes made possible to increase the speed of the morphing flap, reduce the tracking error while restricting stress, temperature and power consumption within very low reasonable levels. The presented numerical results prove the feasibility of a trailing edge morphing section concept triggered by pairs of shape memory alloy antagonistic actuators to achieve meaningful aerodynamic load alleviation in wind turbine blades.

ACKNOWLEDGMENTS

This work has been supported by the INNWIND.EU project, grant No. 308974, funded by the European Union's Seventh Framework Program for research, technological development and demonstration. The Support is greatly appreciated by the authors.

REFERENCES

1. *UpWind Design Limits and solutions for very large wind turbines.* s.l. : Risø National Laboratory - DTU, March 2011.

2. *Trends in the Evolution of Wind Turbine Generator Configurations and Systems.* Thresher, Robert W. and Dodge, Darrell M. 1998, Wind Energy, Vol. 1.

3. Loads amd Structural Stresses. [book auth.] Erich Hau. *Wind Turbines Fundamentals, Technologies, Application, Economics.* s.l. : Springer, 2006, 6.

4. Hansen, Martin O. L. *Aerodynamics of Wind Turbines, Second Edition.* London : Earthscan, 2008.

5. *Combined Analytical/FEA-basec Coupled Aero Structure Simulation of Wind Turbine with Bend-Twist Adaptive Blades.* Maheri, Alireza, Noroozi, Siamak and Vinney, John. s.l. : Elsevier, 2007, Renewable Energy, Vol. 32, pp. 916-930.

6. *Application of Bend-Twist Coupled Blades for Horizontal Axis Tidal Turbines.* Nicholls-Lee, R. F., Turnock, S. R. and Boyd, S. W. s.l. : Elsevier, 2013, Renewable Energy, Vol. 50, pp. 541-550.

7. *Design studies of swept wind turbine blades.* Larwood, Scott, van Dam, C. P. and Schow, Daniel. s.l. : Elsevier, 2014, Renewable Energy, Vol. 71, pp. 563-571.

8. *Passive Load Alleviation Aerofoil Concept with Variable Stiffness multi-stable Composites.* Arrieta, Andres F., et al. s.l. : Elsevier, 2014, Composite Structures, Vol. 116, pp. 235-242.

9. *Review of State of the Art in Smart Rotor Control Research for Wind Turbines.* Barlas, T. K. and van Kuik, G. A. M. 2010, Progress in Aerospace Sciences, Vol. 46, pp. 1-27.

10. *Review of Morphing Concepts and Materials for Wind Turbine Blade Applications.* Lachenal, Xavier, Daynes, Stephen and Weaver, Paul. 2, s.l. : John Wiley & Sons, 2013, Wind Energy, Vol. 16, pp. 283-307.

11. *An Assessment of the Effectiveness of Individual Pitch Contro on Upscaled Wind Turbines.* Chen, Z. J. and Stol, K. A. 2014, Journal of Physics: Conference Series, Vol. 524.

12. *Yaw Systems for wind turbines - Overview of concepts, current challenges and design methods.* Kim, M. G. and Dalhoff, P. H. 2014, Journal of Physics: Conference Series, Vol. 524.

13. *Active Aerodynamic Load Control for Wind Turbine Blades.* Zayas, J. R., et al. Athens, Greece : s.n., 27 February - 2 March 2006. European Wind Energy Conference & Exchibition (EWEC).

14. *Load Alleviation on Wind Turbine Blades using Variable Airfoil Geometry.* Andersen, P. B., et al. Athens, Greece : s.n., 27 February - 2 March 2006. European Wind Energy Conference & Exchibition (EWEC).

15. *Optimal Design of Compliant Trailing Edge for Shape Changing.* Shili, Liu, Wejie, Ge and Shujun, Li. s.l. : Elsevier, 2008, Chinese Journal of Aeronautics, Vol. 21, pp. 187-192.

16. *A Coupled Thermomechanical Beam Finite Element for the Simulation of Shape Memory Alloy Actuators.* Solomou, A., Machairas, T. and Saravanos, D. 7, s.l. : Journal of Intelligent Material Systems and Structures, May 2014, Vol. 25, pp. 809-907.

17. Lagoudas, D. C., [ed.]. *Shape Memory Alloys Modeling and Engineering Applications.* New York : Springer, 2008.

18. *Constitutive Model for the Numerical Analysis of Phase Transformation in Polycrystalline Shape Memory Alloys.* Lagoudas, D., et al. 155-183, 2012, International Journal of Plasticity, Vols. 32-33.

19. *ABAQUS 6.* s.l. : Simulia, 2012. User Subroutines Reference Manual.

20. Bak, C., et al. *Description of the DTU 10 MW Reference Wind Turbine.* Technical University of Denmark. Denmark : DTU Wind Energy, 2013.

21. *Dynamic Stall Modeling on Airfoils based on Strong Viscous-Inviscid Interaction Coupling.* Riziotis, V. A. and Voutsinas, S. G. 2008, Numerical Methods in Fluids, Vol. 56, pp. 185-208.

22. *Flap/Lead-Lag Aeroelastic Stability of Wind Turbine Blades.* Chaviaropoulos, P. K. 2001, Wind Energy, Vol. 4, pp. 183-200.